Shear-strength characteristics of a residual soil

H. Rahardjo, T.T. Lim, M.F. Chang, and D.G. Fredlund

Abstract: Shallow landslides in natural residual soils slopes are common all over the world. The slip surfaces associated with these landslides are often situated above the groundwater table. Therefore, it is important to quantify the contribution of negative pore-water pressure to the shear strength of soil. The shear-strength characteristics of residual soil from the Jurong Formation in Singapore were assessed using multistage, consolidated drained triaxial tests. These tests involved shearing under either a constant net confining pressure and varying matric suctions or under a constant matric suction and varying net confining pressures. An extended form of the Mohr–Coulomb equation was used to interpret the test results. The test results show that for matric suctions up to 400 kPa, the angle of internal friction associated with the matric suction, ϕ^b, is similar to the effective angle of internal friction, ϕ', which averages 26° for the residual soil of the Jurong Formation. The residual soil can maintain a high degree of saturation for matric suctions as high as 400 kPa. Examples involving stability analyses of a residual soil slope with varying pore-water pressure profiles indicate that soil suction contributes significantly to the factor of safety, particularly for shallow slip surfaces.

Key words: residual soil, unsaturated soil, matric suction, shear strength, multistage triaxial test, slope stability.

Résumé : Des glissements superficiels dans des talus de sols résiduels naturels sont fréquents partout dans le monde. Les surfaces de glissement associées à ces mouvements sont souvent localisées au-dessus de la nappe d'eau souterraine. En conséquence, il est important de quantifier la contribution à la résistance au cisaillement de la pression interstitielle négative. Les caractéristiques de la résistance au cisaillement du sol résiduel de la formation du Jurong à Singapour ont été évaluées au moyen d'essais triaxiaux consolidés drainés à étapes multiples. Ces essais impliquaient un cisaillement soit sous une pression nette constante de confinement avec variation des succions matricielles, soit sous une succion matricielle constante avec variation des pressions nettes de confinement. Une forme élargie de l'équation de Mohr–Coulomb a été utilisée pour interpréter les résultats des essais. Les résultats des essais montrent que pour des succions matricielles atteignant jusqu'à 400 kPa, l'angle de frottement interne associé à la succion matricielle, ϕ^b, est semblable à l'angle de frottement interne effectif, ϕ', qui est en moyenne de 26° pour le sol résiduel de la formation de Jurong. Le sol résiduel peut maintenir un haut degré de saturation pour des succions matricielles aussi élevées que 400 kPa. Des exemples comprenant des analyses de stabilité d'un talus de sol résiduel avec différents profils de pression interstitielle indiquent que la succion dans le sol contribue de façon significative au coefficient de sécurité, particulièrement dans le cas des surfaces de glissement peu profondes.

Mots clés : sols résiduels, sol non saturé, succion matricielle, résistance au cisaillement, essai triaxial à étapes multiples, stabilité des talus.

[Traduit par la rédaction]

Introduction

Residual soils are products of the in situ physical and chemical weathering of bedrock. These soils are commonly situated above the groundwater table. Therefore, in situ residual soils are often unsaturated (or approaching saturation) in nature, and the pore-water pressures are negative relative to atmospheric conditions. This negative pore-water pressure is called matric suction when referenced to the pore-air pressure. There has been increasing evidence that matric suction contributes towards the stability of natural slopes in residual soils (Fredlund and Rahardjo 1985). Procedures for slope stability analysis involving negative pore-water pressures have been described by Rahardjo and Fredlund (1991). Therefore, it is of value to quantify the increase in shear strength associated with matric suction.

More than two-thirds of the Singapore land area is covered by residual soils (Pitts 1984). Due to the rapid development on the island, there is an increasing number of

Received September 14, 1993. Accepted August 8, 1994.

H. Rahardjo, T.T. Lim, and M.F. Chang. School of Civil and Structural Engineering, Nanyang, Technological University, Nanyang Avenue, Singapore 2263.

D.G. Fredlund. Department of Civil Engineering, University of Saskatchewan, Saskatoon, SK S7N 0W0, Canada.

Fig. 1. Map of the Nanyang Technological University campus showing the locations of sites IHPT91 and IHPT92.

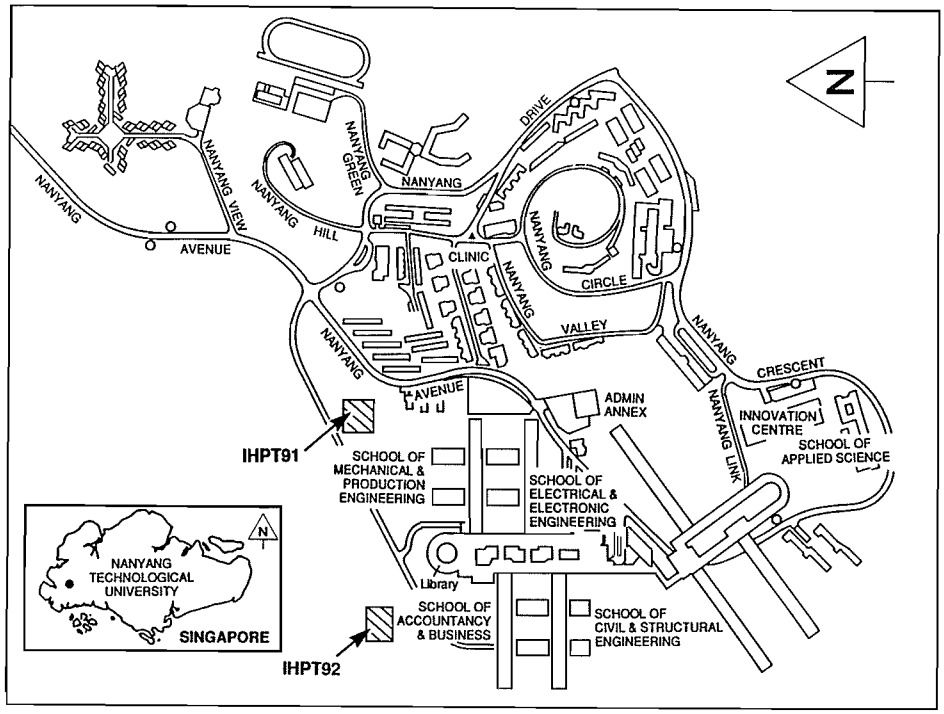

Fig. 2. Generalized profile of residual soil from the sedimentary Jurong Formation at site IHPT91.

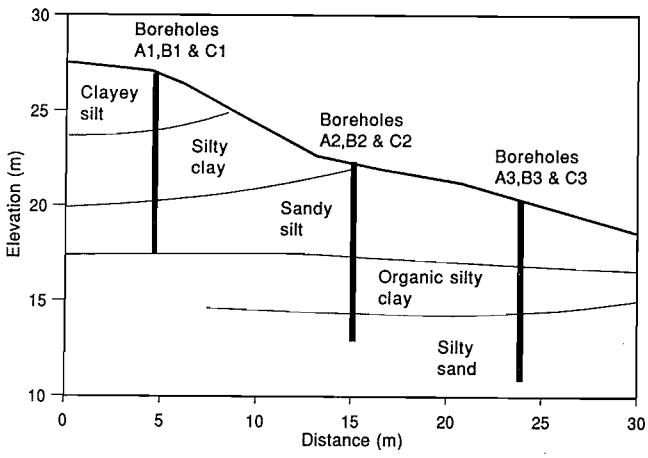

Fig. 3. Generalized profile of residual soil from the sedimentary Jurong Formation at site IHPT92.

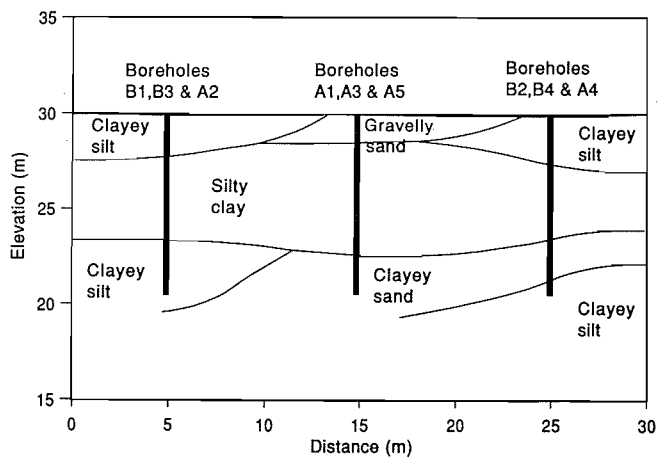

major projects that involve natural residual soils. For instance, on the campus of the Nanyang Technological University (NTU), there are several construction projects underway on its undulating terrain, which is underlain by the residual soil of the sedimentary Jurong Formation. Each of these projects involves a large amount of earthwork and site development.

Although some research has been conducted on Singapore residual soils (i.e., Poh et al. 1985; Yong et al. 1985; Chang 1988; Todo and Pauzi 1989), the shear-strength characteristics of the residual soil of the Jurong Formation are still not well understood. It appears that no attempt has been made to study the effect of matric suction on the shear strength of residual soils of Singapore.

Present and past construction works on the NTU campus have resulted in several slope failures and visible slope movements. Pitts (1985) reported that in the period between 1983 and 1985, a total of 70 landslides had occurred on the NTU campus. Most of these landslides were attributed to continuous precipitation that eventually caused the soil suction to decrease to the point where a mass of soil could slide. These slides have prompted a more in-depth study of the behavior of the natural residual soils, particularly with consideration of the effect of soil suction.

A knowledge of how soil suction influences the shear strength of soil enables an engineer to take its influence into consideration in designs related to slopes. Concerns related to slope surface protection works, such as provision

Fig. 4. Variation of soil properties with depth at site IHPT91. SPT N value standard penetation test number of blows per 30 cm penetration; RST N_{20}, Swedish ram sounding test number of blows per 20 cm penetration.

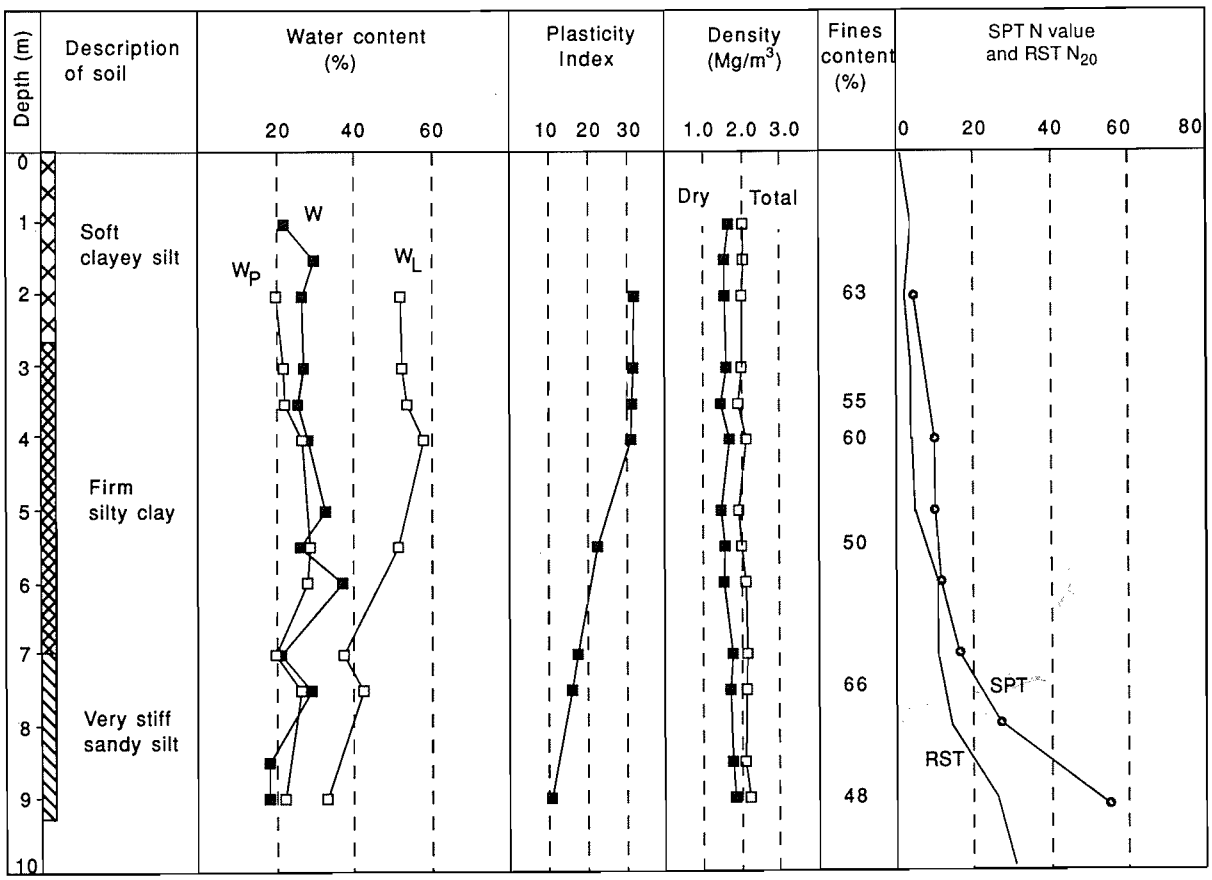

for surface drainage and the covering of fresh cut slopes with waterproof sheets, can be addressed in a more rational manner through an understanding of the effects of a matric-suction change.

The shear-strength theory for an unsaturated soil takes the form of an extended Mohr–Coulomb envelope (Fredlund et al. 1978), which can be used to evaluate the contribution of matric suction on the shear strength. The effective shear strength parameters were measured for the Jurong Formation residual soil using multistage consolidated drained triaxial tests in a modified triaxial test apparatus based on the axis-translation technique (Hilf 1956).

Site conditions and general soil properties

The influence of negative pore-water pressures on the behavior of an unsaturated soil depends on the soil type. Consideration of the general properties of the soil will assist in the interpretation of the results from triaxial tests.

Site condition and field investigation

The soils investigated are from two sites on the NTU campus. Their locations are shown in Fig. 1 as IHPT91 and IHPT92, which are about 300 m apart. Site IHPT91 is on a slope with an inclination of 18°. Site IHPT92 is on flat ground. A total of nine boreholes, spaced at 10 m centers in a square grid, were drilled at each site. According to the geology map of Singapore, both sites are underlain by the residual soil of the Jurong Formation. Borehole logs obtained from the sites indicate that subsoils at the two sites have similar stratigraphy. The generalized cross sections of the soil profiles at the sites are shown in Figs. 2 and 3. The soils generally consist of silty sand, sand or clayey silt, and silty clay.

Undisturbed samples were recovered using 75 mm diameter thin-wall Shelby tubes with an area ratio of approximately 10%. The samples were of good quality and were used for laboratory shear strength tests. Disturbed samples were also collected during the standard penetration tests for index properties tests. Swedish ram sounding tests (RST) were also performed next to each borehole at both sites. The RST involves driving a conical tip with an apex angle of 90°, a diameter of 45 mm, and a length of 90 mm, using a 64.5 kgf (kilogram force) hammer dropped freely from a height of 500 mm (Chang 1988). These tests indicated that the consistency and density of the soil generally increased with depth.

General soil properties

Figures 4 and 5 show the variation of the subsoils and their properties with depth at sites IHPT91 and IHPT92. There is similarity between the properties profiles at the two test sites. The measured liquid limits are generally between

Fig. 5. Variation of soil properties with depth at site IHPT92.

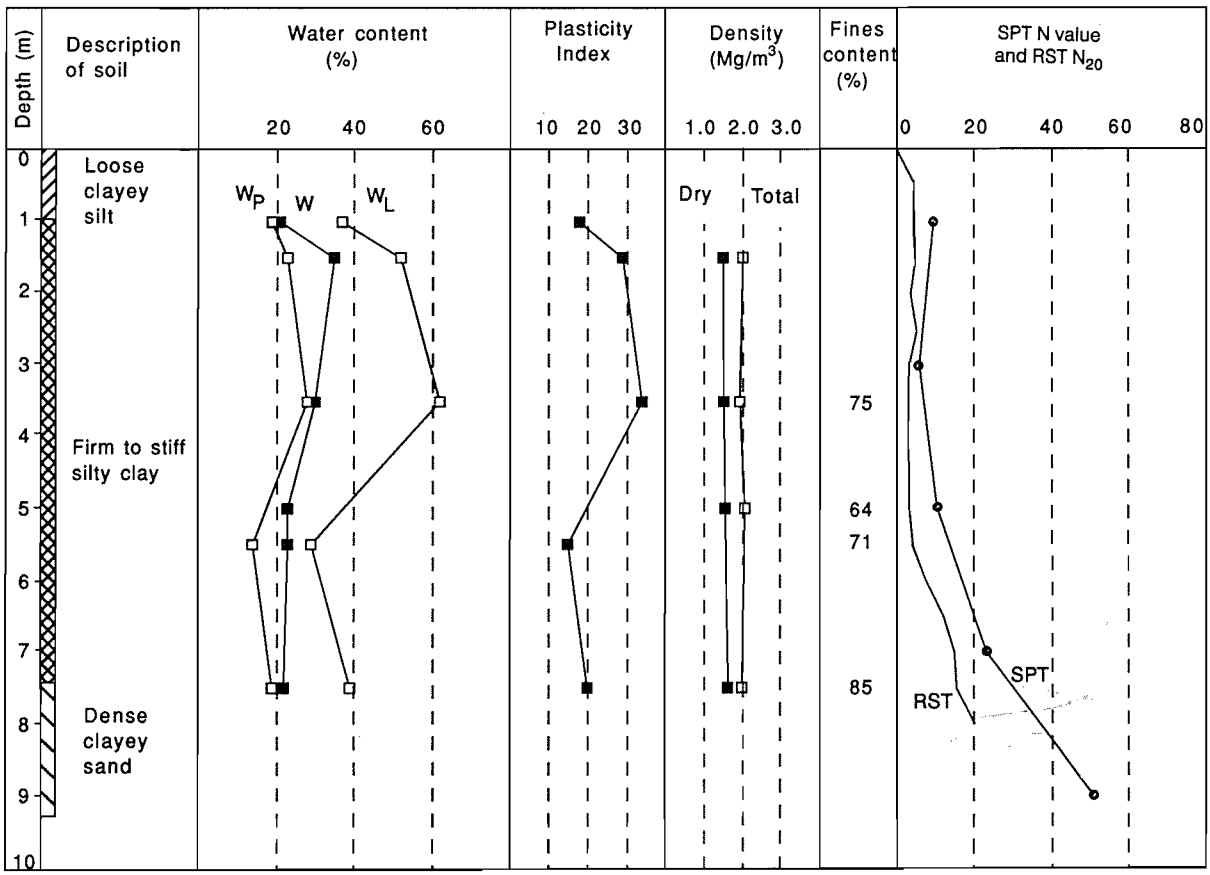

30 and 60, and the plastic limits are between 15 and 30. The plasticity index ranges from 10 to 35. Therefore, the soils are of medium to high plasticity. The water content is more or less constant within a depth of 9 m below the ground surface. In general, the plasticity index decreases with depth.

The grain-size distribution of a residual soil depends on the degree of weathering and the composition of its parent material. Results presented by Pitts (1985) and Yong et al. (1985) and results from the present investigation show a significant variability in the grain-size distribution for the residual soil from the Jurong Formation. The fines content (i.e., percent finer than the No. 200 sieve size) for the residual soil ranges from 48 to 66% at site IHPT91 and from 64 to 85% at site IHPT92.

The total density and dry density increase marginally with depth, and their average values are about 2.05 and 1.67 Mg/m^3, respectively. The specific gravity is 2.68, with a standard deviation of 0.008. This value is higher than those of quartz, kaolinite, and feldspar because of the presence of iron minerals.

Yong et al. (1985) conducted X-ray diffraction tests on four samples from the residual soils of the Jurong Formation. The X-ray diffractogram obtained from air-dried specimens and also from specimens heated to 550°C indicated the presence of a plagioclase feldspar, quartz, mica and kaolinite. The predominant clay mineral in the residual soil is kaolinite.

Shear-strength theory for soils with suction

The unsaturated soil shear-strength theory, in the form of an extended Mohr–Coulomb envelope, as proposed by Fredlund et al. (1978) is used as a basis for the interpretation of the data. The proposed equation is as follows:

$$[1] \quad \tau_{ff} = c' + (\sigma_f - u_a)_f \tan \phi' + (u_a - u_w)_f \tan \phi^b$$

where

c' is intercept of the "extended" Mohr–Coulomb failure envelope on the shear-stress axis where the net normal stress and the matric suction at failure are equal to zero; it is also referred to as effective cohesion;

$(u_a - u_w)_f$ is matric suction on the failure plane at failure, where u_a is pore-air pressure and u_w pore-water pressure;

$(\sigma_f - u_a)_f$ is net normal stress state variable on the failure plane at failure;

ϕ' is angle of internal friction associated with the net normal stress state variable $(\sigma_f - u_a)_f$; and

ϕ^b is angle indicating the rate of increase in shear strength relative to matric suction, $(u_a - u_w)_f$.

The above equation, which is an extended form of the Mohr–Coulomb equation, defines a planar surface. The Mohr circles corresponding to failure conditions can be plotted on a three-dimensional graph. The three-dimensional plot has the shear stress, τ, as the ordinate and the two stress-state variables, $(\sigma - u_a)$ and $(u_a - u_w)$, as abscissas,

Fig. 6. Extended Mohr–Coulomb failure envelope for soils with matric suction.

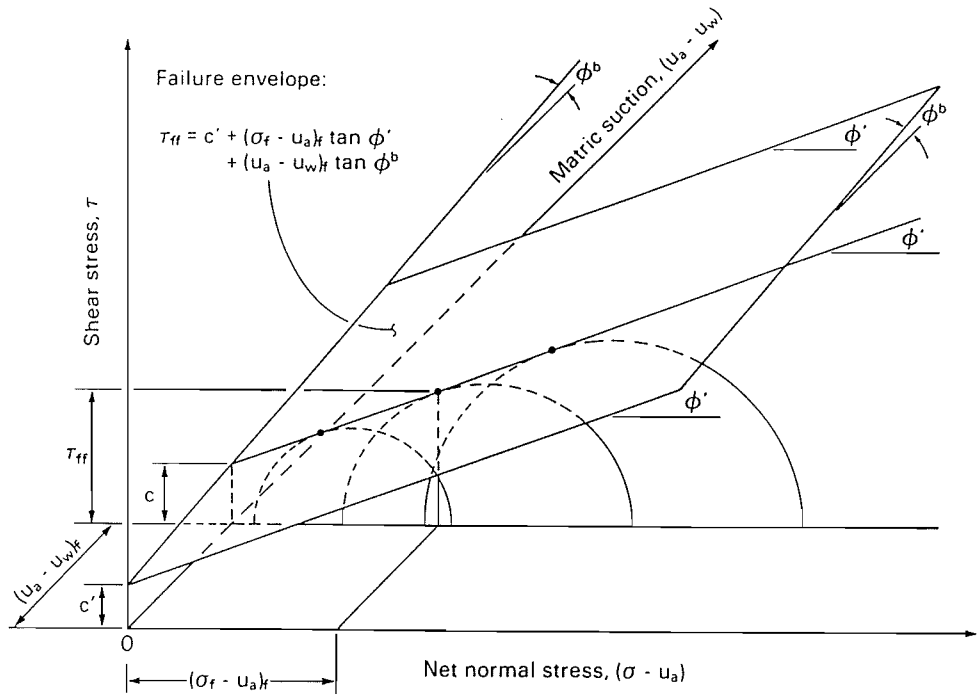

as shown in Fig. 6. The frontal plane represents the failure envelope for a saturated condition where the matric suction is zero. On the frontal plane, the $(\sigma - u_a)$ axis reverts to the $(\sigma - u_w)$ axis, since the pore-water pressure becomes equal to the pore-air pressure at zero matric suction. Therefore, there is a smooth transition in the shear-strength equation when moving from an unsaturated condition (eq. 1) to a saturated condition. The failure envelope intersects the shear stress versus matric suction plane along a line of intercepts as shown in Fig. 6. The equation for the line of intercept is as follows:

$$[2] \quad c = c' + (u_a - u_w)_f \tan \phi^b$$

where c is ordinate intercept of the extended Mohr–Coulomb failure envelope on the shear stress versus matric suction plane.

The extended Mohr–Coulomb failure envelope may be planar or somewhat curved. The proposed theory assumes the failure envelope is planar and can be described by [1].

Alternatively, if the top point of a Mohr circle at failure (i.e., coordinates p_f, q_f, r_f) is used to describe the stress conditions at failure, a stress-point envelope can be drawn through the stress points at failure. The stress-point envelope, which is an extended form of the p–q diagram proposed by Lambe and Whitman (1979), is shown in Fig. 7. The envelope can be defined as follows (Fredlund and Rahardjo 1993*b*):

$$[3] \quad q_f = d' + p_f \tan \psi' + r_f \tan \psi^b$$

where

q_f is half of the deviator stress at failure (i.e., $(\sigma_1 - \sigma_3)_f/2$);
σ_{1f} is major principal stress at failure;
σ_{3f} is minor principal stress at failure;
d' is intercept of the stress-point envelope on the q axis when p_f and r_f are equal to zero;
$p_f = [(\sigma_1 + \sigma_3)_f/2 - u_a]_f$, which is net normal stress at failure;
ψ' is slope angle of the stress-point envelope with respect to the stress variable p_f;
r_f is matric suction at failure (i.e., $(u_a - u_w)_f$); and
ψ^b is slope angle of the stress-point envelope with respect to the stress variable r_f.

Similar to the extended Mohr–Coulomb failure envelope, the equation for the line of intercept on q versus r plane can be written as follows:

$$[4] \quad d = d' + r_f \tan \psi^b$$

where d is ordinate intercept of the stress-point envelope on the q versus r plane.

The variables d, d', ψ', and ψ^b in [3] and [4] can be related to the parameters c, c', ϕ', and ϕ^b of the extended Mohr–Coulomb failure envelope as follows:

$$[5] \quad \tan \psi' = \sin \phi'$$

$$[6] \quad d = c \cos \phi'$$

$$[7] \quad d' = c' \cos \phi'$$

$$[8] \quad \tan \psi^b = \tan \phi^b \cos \phi'$$

Either form of failure envelope can be used for the interpretation of results from the unsaturated soil triaxial tests.

Test program and triaxial test procedure

The laboratory testing program involved the use of a conventional triaxial cell modified for both air- and water-pressure control (Fredlund and Rahardjo 1993*b*). The

Fig. 7. Stress-point envelope for soils with matric suction.

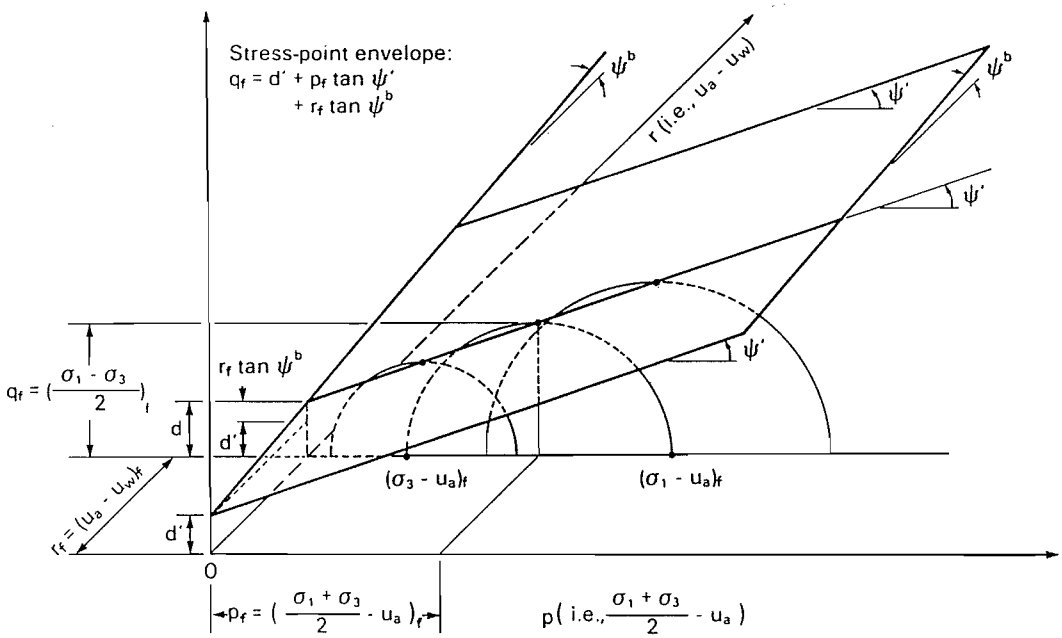

Fig. 8. Modified triaxial cell for testing soil specimens under various matric suctions using the axis-translation technique.

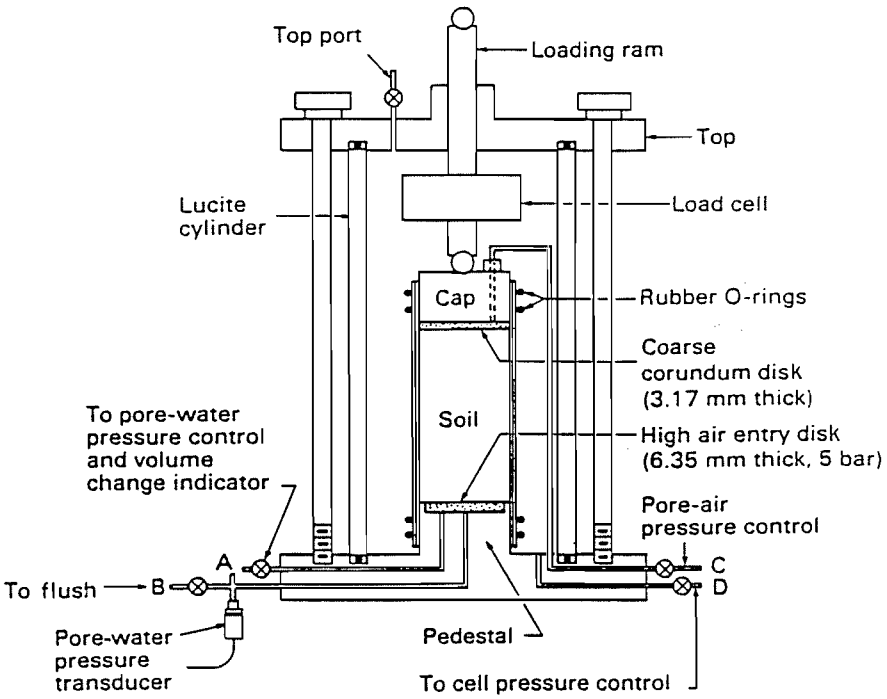

modified triaxial cell is shown in Fig. 8. The-axis translation technique (Hilf 1956) was used to apply the desired matric suction values. A 5 bar (1 bar = 100 kPa) high-entry disk sealed onto the bottom pedestal of the modified apparatus was used to facilitate a separate control of the pore-air and pore-water pressures.

A total of 12 soil specimens were prepared from undisturbed samples obtained from sites IHPT91 and IHPT92. Descriptions of the soil specimens used in the test program are summarized in Table 1. Except for specimen S3-91, which was classified as a firm clayey silt, all the other 11 specimens were classified as stiff silty clay. Multistage triaxial tests were conducted to minimize the effect of variability of the specimens on the test results. Two testing procedures were used (Lim 1994): (*i*) multistage triaxial tests at a constant net confining pressure ($\sigma_3 - u_a$), for various matric suctions ($u_a - u_w$); and (*ii*) multistage triaxial tests at a constant matric suction ($u_a - u_w$), for various

Table 1. Summary of undisturbed samples used in the triaxial test program.

Borehole No.	Location	Sample No.[a]	Depth (m)	Triaxial test No.[b]	SPT[c] *N* value (blows/30 cm)	Description
A1	IHPT91	UD2-91	3.00–3.15	S2-91	11	Stiff yellowish-orange sandy silty clay
A1	IHPT91	UD2-91	3.15–3.30	U1-91		
A1	IHPT91	UD2-91	3.30–3.45	U2-91		
A1	IHPT91	UD2-91	3.45–3.60	U3-91		
C2	IHPT91	UD1-91	1.25–1.40	S3-91	4	Firm yellowish-grey sandy clayey silt
A1	IHPT92	UD3-92	5.55–5.70	S1-92	14	Stiff reddish-brown sandy silty clay
A1	IHPT92	UD3-92	5.40–5.55	U1-92		
A1	IHPT92	UD3-92	5.25–5.40	U2-92		
A1	IHPT92	UD4-92	7.00–7.15	S2-92	12	Stiff yellowish-brown sandy silty clay
A1	IHPT92	UD4-92	7.15–7.30	U4-92		
B2	IHPT92	UD2-92	3.55–3.70	S3-92	8	Stiff reddish-brown silty clay
B2	IHPT92	UD3-92	5.30–5.45	S4-92	10	Stiff yellowish-brown sandy silty clay

[a]UD indicates undisturbed samples retrieved from 75 mm diameter thin-wall Shelby tubes.
[b]S, triaxial test with $(u_a - u_w) = 0$; U, triaxial test with $(u_a - u_w) > 0$.
[c]SPT, standard penetration test.

net confining pressures $(\sigma_3 - u_a)$. All the test specimens were 71 mm in diameter and 142 mm in height.

Multistage consolidated drained (CD) tests were conducted on all specimens. The test began with an initial saturation of the test specimen. During saturation, a nominal effective confining pressure of 10 kPa was applied. The residual soil has low swelling characteristics (i.e., swelling pressure about 5–10 kPa). Due to the hysteresis associated with the wetting and drying curves (i.e., water content versus matric suction relationship), all the specimens were tested following a path of decreasing water content (i.e., increasing matric suction or increasing net confining pressure at successive stages). In the consolidation stage, the specimen was consolidated under an isotropic confining pressure σ_3, a pore-air pressure u_a, and a pore-water pressure u_w. A constant net confining pressure and a constant matric suction were maintained during the shearing process. A low shearing rate of 0.0009 mm/min was adopted to maintain drained conditions for both the air and water phases (Lim 1994). A "cyclic" loading procedure was adopted (Fredlund and Rahardjo 1993*b*). The deviator stress was applied until it was apparent that the deviator stress was approaching a peak value. At this point, the vertical load was removed and a new stress state was applied for a subsequent stage of loading. A total of three to five stages of loading was applied to each specimen.

A study was also made of the soil-water characteristic curves of the residual soil. A 5 bar Pressure Plate Extractor (Soilmoisture Equipment Inc., Santa Barbara, Calif.) was used for applying the desired matric suction values to the specimens. Two specimens from site IHPT91 and three specimens from site IHPT92 were selected. All specimens were trimmed from undisturbed samples recovered from the silty clay soil strata. The diameter and height of the specimens were 71 and 27 mm, respectively. The soils used for the determination of the soil-water characteristic curve were the same as the soils used in the triaxial tests.

The test was commenced by saturating the specimen with deaired water. A low suction value (i.e., 40 kPa) was first applied to the specimen. The pore water in the specimen was squeezed out in response to the applied suction value. The weight of each specimen was recorded at selected intervals during each applied suction. When the weight of the specimen remained constant with respect to time (i.e., in equilibrium conditions), the weight and the dimension of the specimen were recorded. Higher matric suction values were then applied to the specimen until a maximum value of 500 kPa suction was achieved. The dry weight of the specimen was obtained by oven drying of the specimen at the end of test. As a result, the water content, void ratio, and degree of saturation of the specimen in equilibrium with each applied suction could be calculated. The plotted soil-water characteristic curves (for the drying process) show the desaturation characteristics of the specimens.

Typical test results and their interpretation

Figures 9 to 11 show the deviator stress and water volume change versus strain curves associated with the multistage triaxial tests under constant matric suctions, and under constant net confining pressures. These curves indicated that the peak deviator stress increases with subsequent loadings of increased matric suction or increased net confining stress. The soil stiffness increases from the first stage to the second stage (which is a typical behavior of fine-grained soils) and then remains more or less unchanged at subsequent stages. Similar shear stress development and

Fig. 9. Deviator stress and water volume change vs. axial strain curves from a test conducted at zero matric suction (triaxial test S3-91).

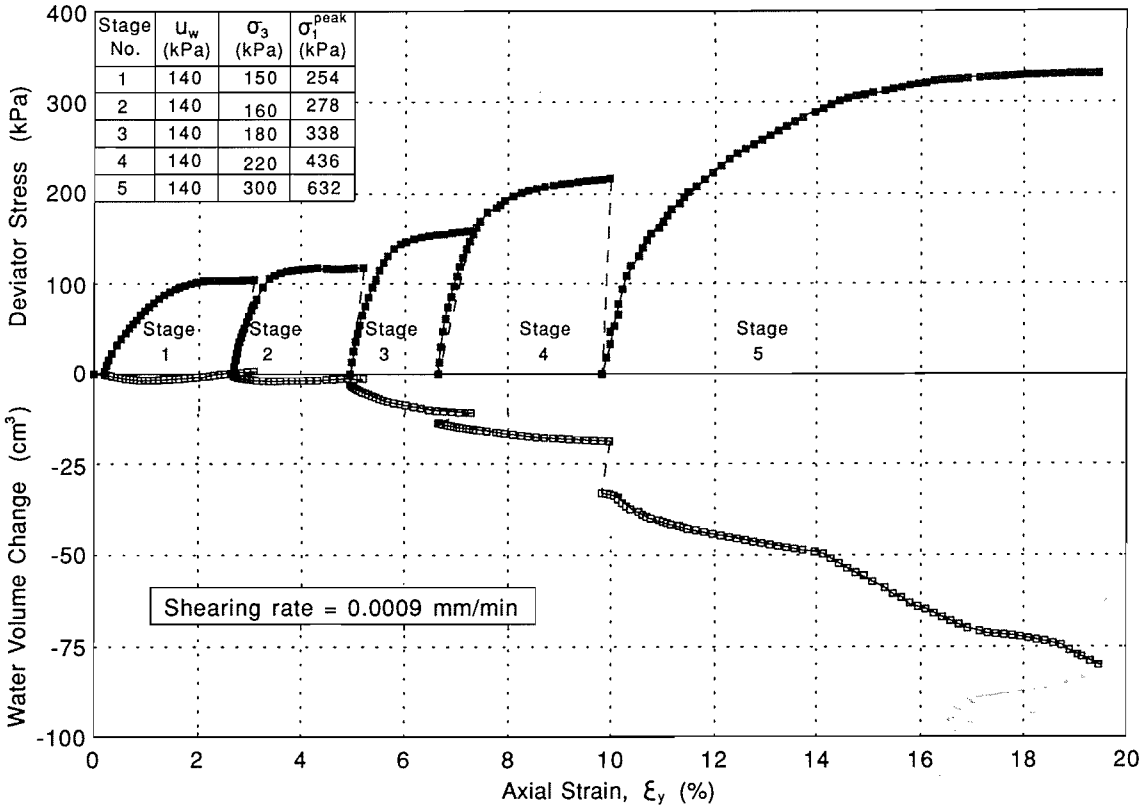

water volume change behavior can be observed in both test procedures involving increasing net confining pressures and increasing matric suctions.

The stress conditions at peak strength during the multistage triaxial tests are summarized in Tables 2 and 3 for all the test specimens. The Mohr circles corresponding to failure conditions can be plotted on a three-dimensional graph. Either an extended Mohr–Coulomb failure envelope or a stress-point envelope can be used to analyze the results. The stress-point envelope was used to determine the d', d, and ψ' parameters. These parameters were then converted to c', c, and ϕ'. The ϕ^b value was then interpreted from the extended Mohr–Coulomb failure envelope using the ϕ' value corresponding to the computed ψ'.

Determination of ϕ' and c'

A knowledge of the effective angle of internal friction, ϕ', and the effective cohesion, c', is necessary to define the value of ϕ^b in [1]. The procedure adopted here is described by Fredlund and Rahardjo (1993*b*). A regression line through the stress-point envelopes with coordinates (p_f, q_f, r_f) was used to represent the stress conditions at failure. Figure 12 shows plots of stress-point envelopes for some selected test results. The stress-point envelope was defined in [3]. The slope of the envelope, tan ψ', and the intercept, d (or d' when matric suction is equal to 0) can be computed using a least-squares method. The coefficient of correlation between the p_f and q_f coordinates was computed. Using [5]–[7], the c (or c' when matric suction is equal to 0) and ϕ' parameters describing the extended Mohr–Coulomb envelope can be determined.

Table 4 summarizes the results obtained from plots of the stress-point envelopes for all tests conducted at a constant matric suction. The coefficient of correlation is close to 1.0. The interpreted ϕ' values are quite consistent at various matric suction values (0, 200, and 300 kPa in tests S1-92, U1-92, and U2-92). For test U2-92, the ϕ' value is slightly lower. This is probably due to some "overshearing" of the specimen in the second stage, which subsequently caused a lower peak strength in the third stage. In general, the ϕ' value was 26 ± 1°. The interpreted c' value varied from 30 to 45 kPa, with values as low as 19 kPa. The variation in the effective cohesion, c', is believed to be associated with variations in the fines content, sesquioxides content (i.e., iron oxides and aluminum oxide), and aging effects in the samples. Although the effective cohesion measurements are quite high, the values are typical of residual soils.

Determination of ϕ^b

The value of ϕ^b for the soil was interpreted from results of triaxial tests conducted at various matric suction values. If a constant friction angle ϕ' of 26° is assumed over the range of matric suction from 0 to 400 kPa, the failure envelope can be drawn tangent to each Mohr circle at a specific matric suction. A typical set of results from the multistage test at a constant net normal stress but varying matric suction values (i.e., test U4-92) is shown in Fig. 13.

Fig. 10. Deviator stress and water volume change vs. axial strain curves from multistage tests at a constant net confining pressure for various matric suctions. (*a*) Triaxial test U1-91. (*b*) Triaxial test U2-91.

(a)

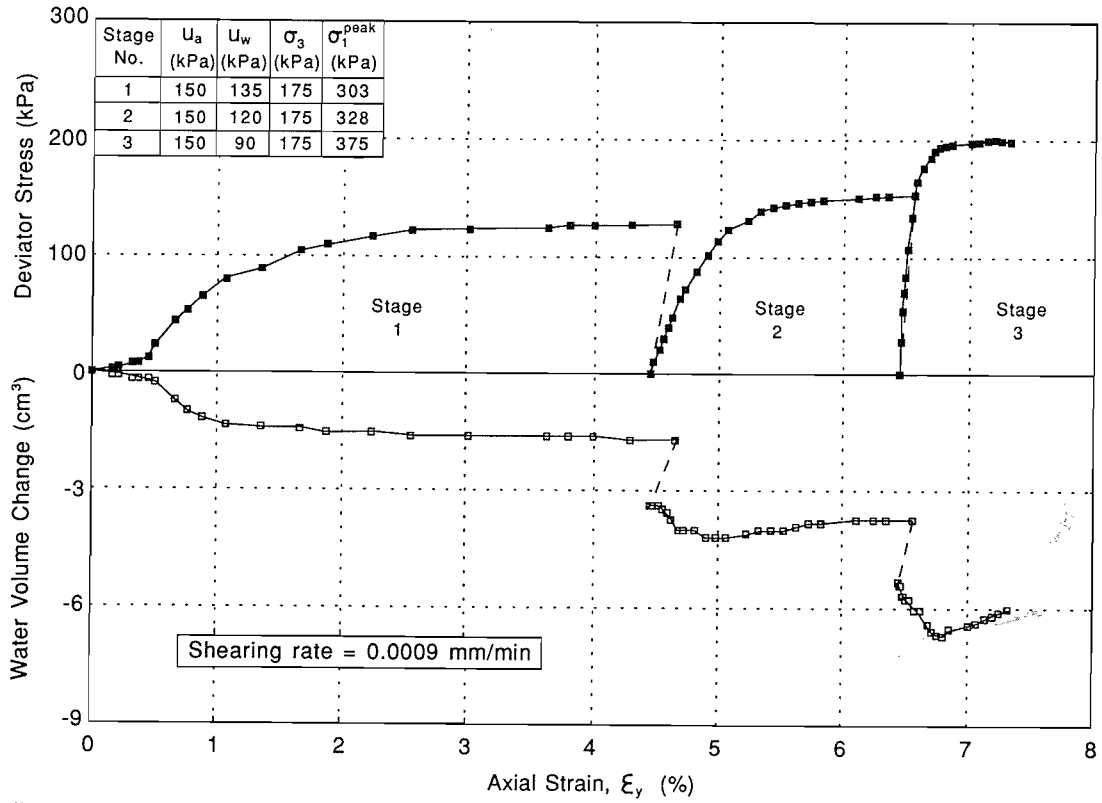

(b)

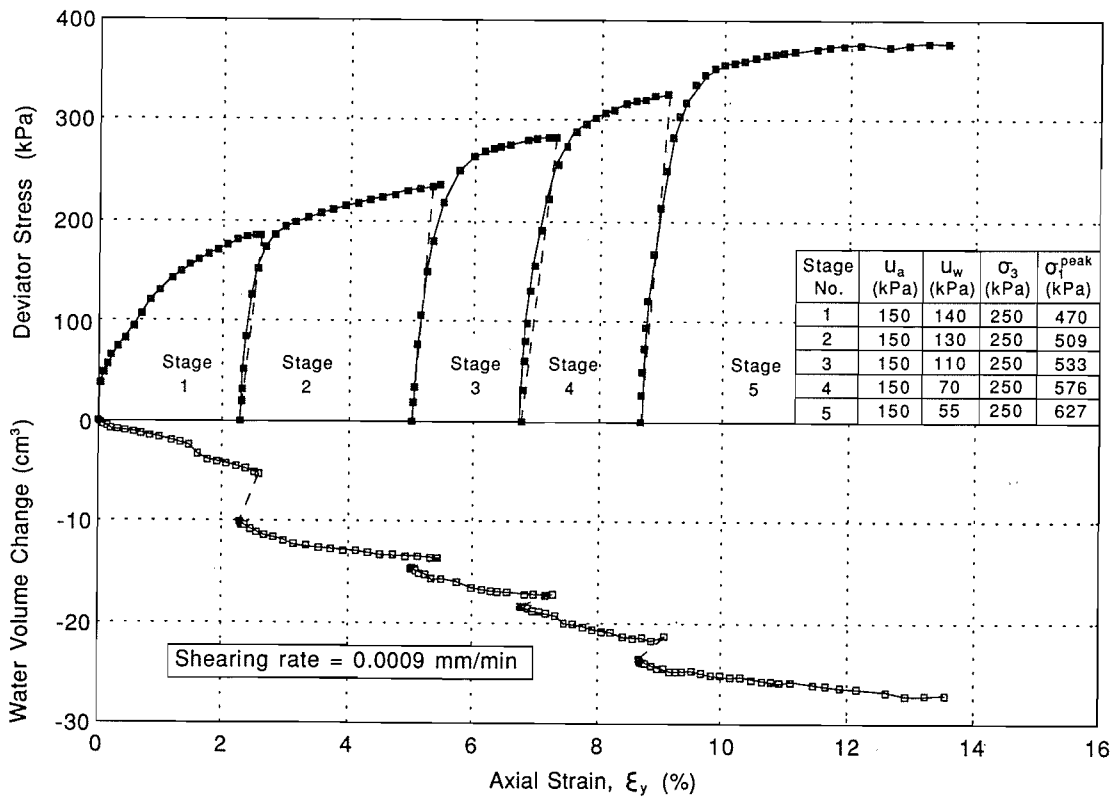

Fig. 10. (*concluded*) (*c*) Triaxial test U3-91. (*d*) Triaxial test U4-92.

(c)

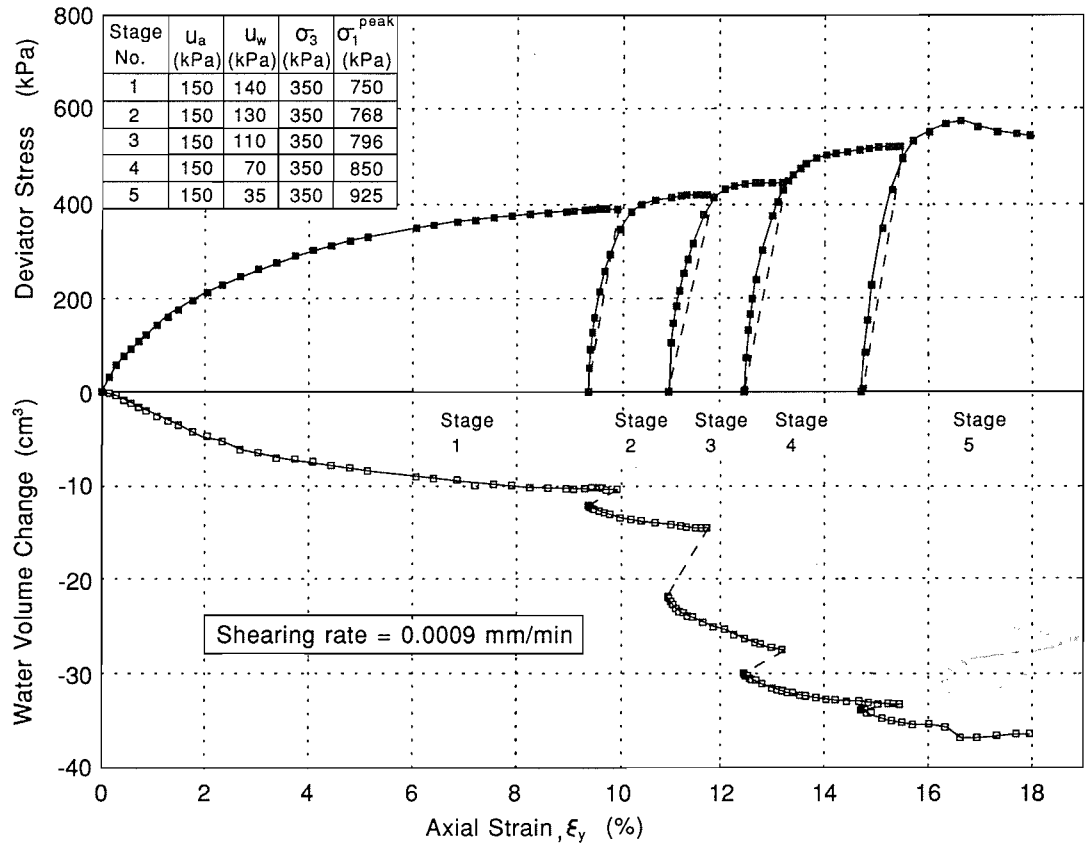

(d)

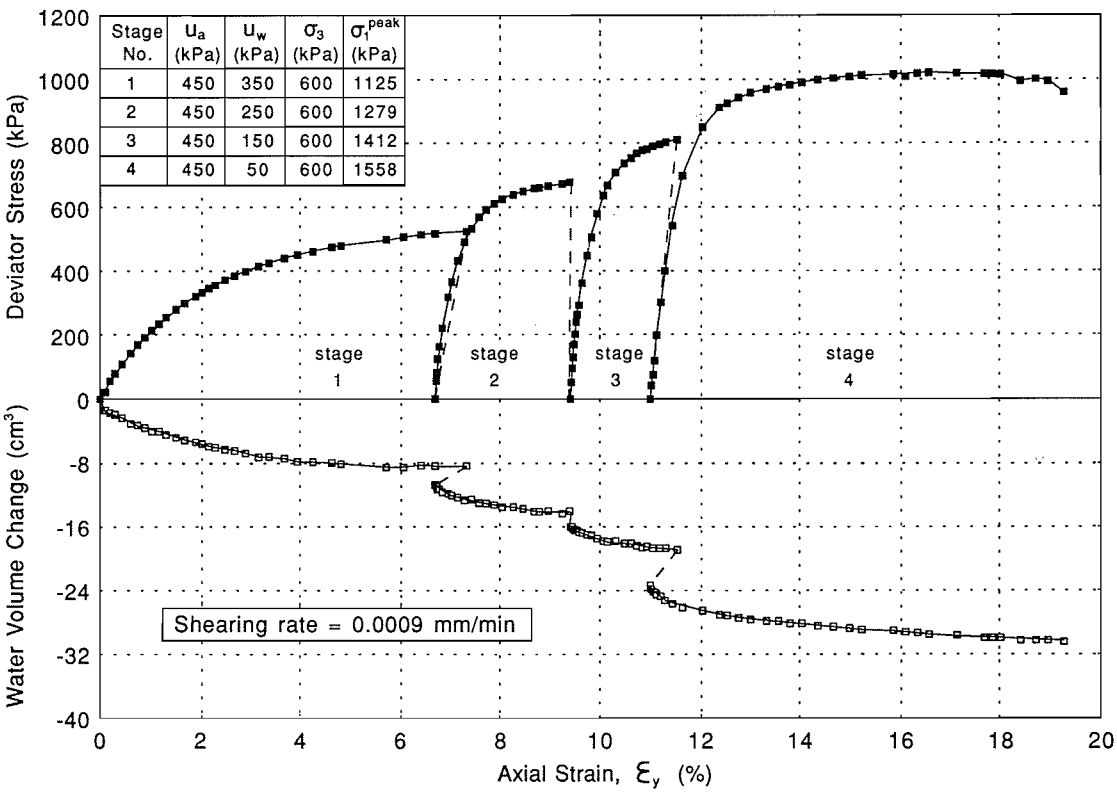

Fig. 11. Deviator stress and water volume change vs. axial strain curves under constant matric suction for residual sedimentary soil of the Jurong Formation. (*a*) Triaxial test U1-92. (*b*) Triaxial test U2-92.

(a)

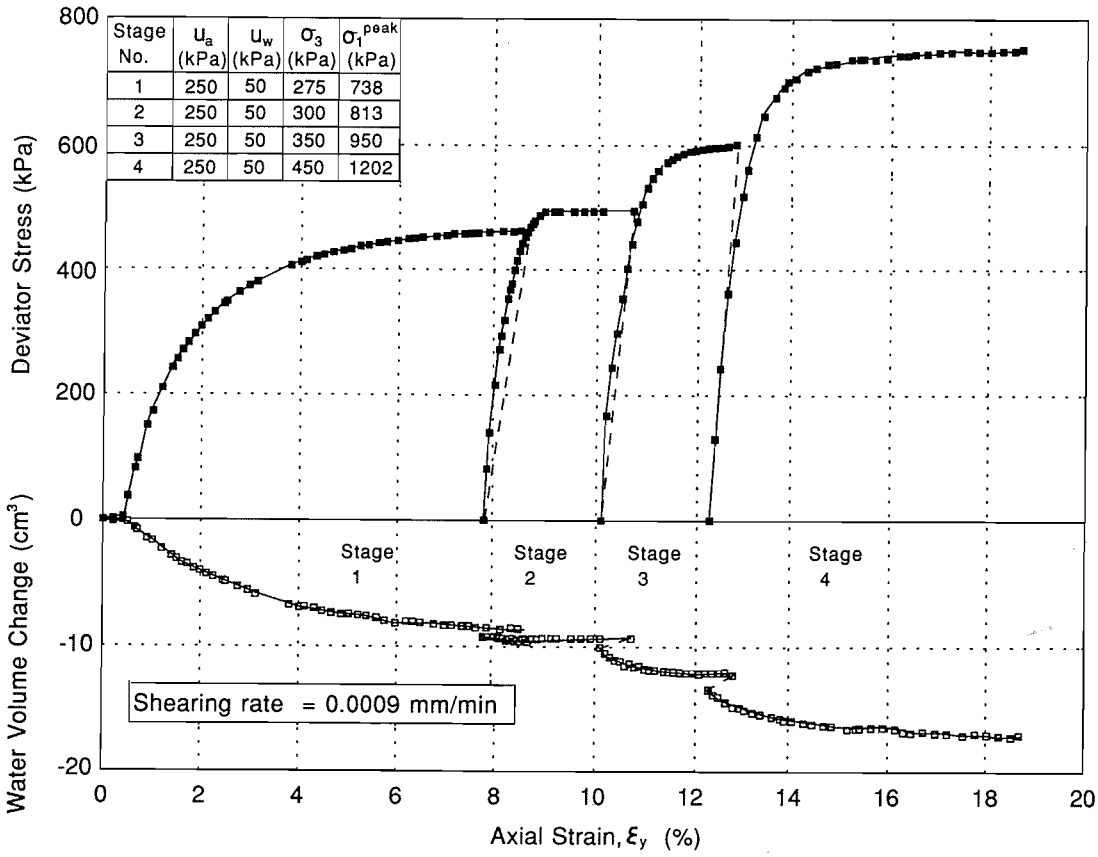

(b)

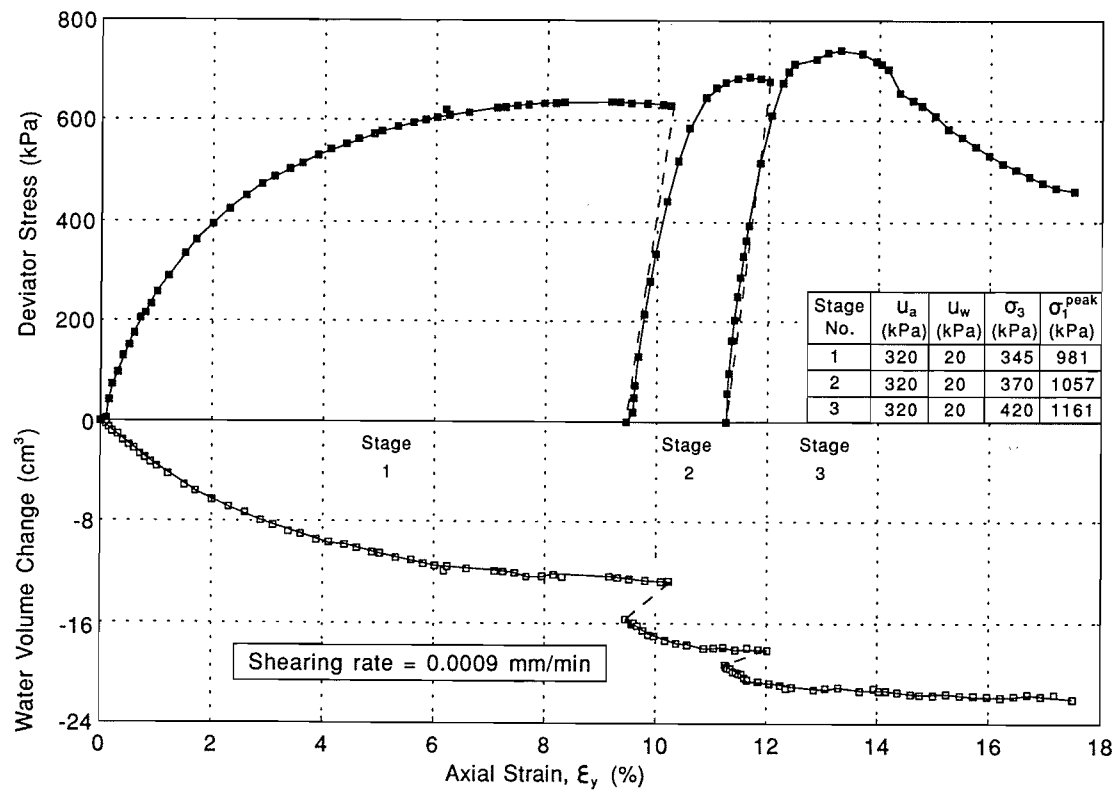

Table 2. Stresses at failure measured in multistage triaxial tests at matric suction equal to zero.

Triaxial test No.	Stage No.	u_w (kPa)	σ_3 (kPa)	σ_1^{peak} (kPa)	$\sigma_3 - u_w$ (kPa)	$\sigma_1 - u_w$ (kPa)
S2-91	1	140	155	231	15	91
	2	140	165	269	25	129
	3	140	240	440	100	300
	4	140	340	695	200	555
S3-91	1	140	150	254	10	114
	2	140	160	278	20	138
	3	140	180	338	40	198
	4	140	220	436	80	296
	5	140	300	632	160	492
S1-92	1	140	190	360	50	220
	2	140	240	510	100	370
	3	140	290	636	150	496
	4	140	340	756	200	616
S2-92	1	190	240	428	50	238
	2	190	290	537	100	347
	3	140	290	617	150	477
	4	140	340	769	200	629
S3-92	1	190	215	372	25	182
	2	190	240	452	50	262
	3	190	290	567	100	377
	4	190	340	697	150	507
S4-92	1	190	390	854	200	664
	2	190	440	990	250	800
	3	190	490	1120	300	930
	4	190	540	1245	350	1055

The total cohesion intercept c at each matric suction was determined from the point where the failure envelope intersects the shear stress versus matric suction plane. Figure 14 presents a plot of the best-fit straight line through the cohesion intercepts at various matric suction values for each of the tests. The lines of intercept indicate an increase in strength as the matric suction increases. The equation for the best-fit line of the cohesion intercepts is as given in [2].

The values for ϕ^b obtained from the multistage triaxial tests in Fig. 14 are summarized in Table 5. The average value is about 26° for matric suctions up to 400 kPa, which is the same as the value of ϕ'. An investigation on the sample types used in the triaxial tests indicated that even at a matric suction of 400 kPa, the soil specimens still remain essentially saturated. This can be seen from the soil-water characteristic curves for the silty clay specimens (Fig. 15). At or near saturation conditions, the air phase consists of a few occluded bubbles. The soil would be expected to behave essentially as though it were saturated. In other words, the negative pore-water pressure acts throughout the pores as in a saturated soil. Consequently, an increase in matric suction produces the same increase in shear strength as does an increase in net normal stress. As a result, essentially the same values are obtained for the friction angles ϕ' and ϕ^b. A planar failure plane is therefore suitable for defining the failure conditions of the residual soil from the Jurong Formation for the stress state range studied.

Incorporation of matric suction in slope stability analysis

Landslides in steep residual soil slopes are common in tropical regions. Their occurrences often follow periods of prolonged heavy rains. Cases of landslides in Brazil (Vargas and Pichler 1957), southeast Asia (Brand 1984), Japan (Oyaga 1984), and many other countries have been reported. Shallow landslides are the most common form of mass movement in residual soil areas, and failure most commonly comes during or after heavy rains. The landslides are generally 3–5 m deep, and the failure surfaces are usually parallel to the slope surface. Although this form of failure usually does not result in great disasters and casualties, they can, however, amount to considerable losses. A typical case history of a shallow landslide in residual soils in Santos, Brazil, was reported by Vargas and Pichler (1957). The translational slide was produced by a shallow sliding mass of residual soils, along fissured blocks of partially decomposed rock. The angle of the slope before slippage was 42°, and the slide extended to a length of about 100 m upslope. An analysis of the causes of the slide indicated that prolonged heavy rainfall was the main reason. It was believed that the infiltration of rainwater destroyed the suction that had kept the slope stable before the slide.

The following analysis illustrates how the factor of safety of a slope is affected by the matric suction in the

Table 3. Stresses at failure measured in multistage triaxial tests at matric suction greater than zero.

Triaxial test No.	Stage No.	u_w (kPa)	u_a (kPa)	σ_3 (kPa)	σ_1^{peak} (kPa)	$\sigma_3 - u_w$ (kPa)	$\sigma_1 - u_w$ (kPa)	$u_a - u_w$ (kPa)
U1-91	1	135	150	175	303	25	153	15
	2	120	150	175	328	25	178	30
	3	90	150	175	375	25	225	60
U2-91	1	140	150	250	470	100	320	10
	2	130	150	250	509	100	359	20
	3	110	150	250	533	100	383	40
	4	70	150	250	576	100	426	80
	5	55	150	250	627	100	477	95
U3-91	1	140	150	350	750	200	600	10
	2	130	150	350	768	200	618	20
	3	110	150	350	796	200	646	40
	4	70	150	350	850	200	700	80
	5	35	150	350	925	200	775	115
U1-92	1	50	250	275	738	25	488	200
	2	50	250	300	813	50	563	200
	3	50	250	350	950	100	700	200
	4	50	250	450	1202	200	952	200
U2-92	1	20	320	345	981	25	661	300
	2	20	320	370	1057	50	737	300
	3	20	320	420	1161	100	841	300
U4-92	1	350	450	600	1125	150	675	100
	2	250	450	600	1279	150	829	200
	3	150	450	600	1412	150	962	300
	4	50	450	600	1558	150	1108	400

Fig. 12. Results of multistage triaxial tests and their corresponding stress-point envelopes.

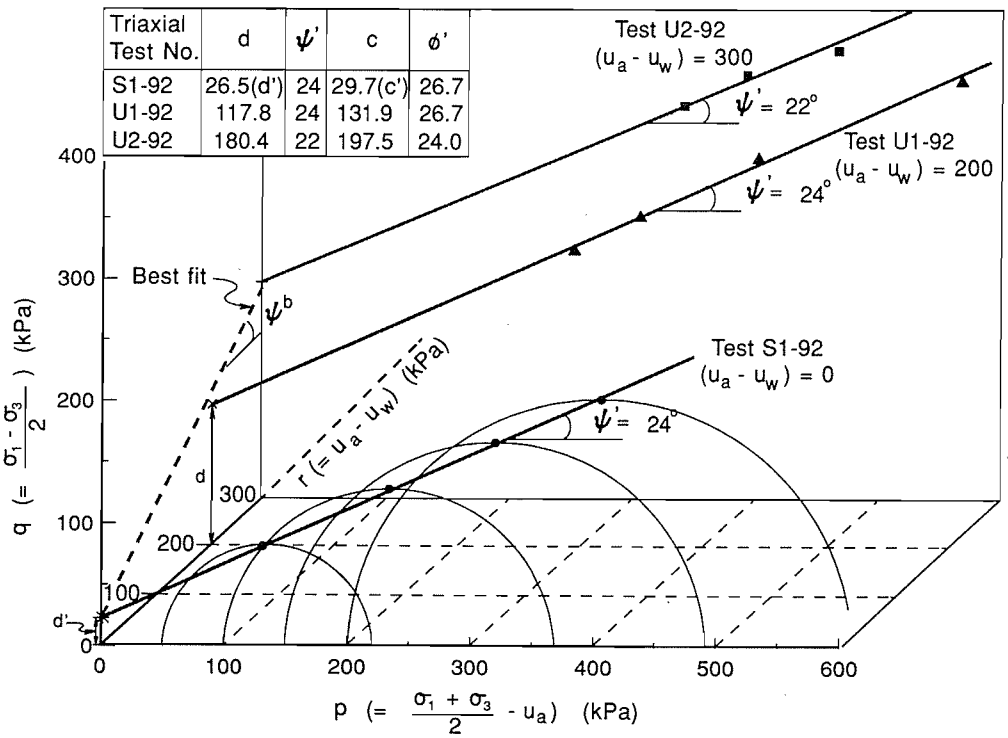

Table 4. Summary of c' and ϕ' values interpreted from triaxial tests.

Borehole No.	Location	Sample No.	Depth (m)	Triaxial Test No.	Shear-strength parameters c' (kPa)	c (kPa)	ϕ' (°)	Correlation coefficient	Description of test
A1	IHPT91	UD2-91	3.00–3.15	S2-91	18.7		25.1	0.999	Multistage (4 stages) at constant matric suction = 0 kPa
C2	IHPT91	UD1-91	1.25–1.40	S3-91	28.9		25.6	0.999	Multistage (5 stages) at constant matric suction = 0 kPa
A1	IHPT92	UD3-92	5.55–5.70	S1-92	29.7		26.7	0.999	Multistage (4 stages) at constant matric suction = 0 kPa
A1	IHPT92	UD3-92	5.40–5.55	U1-92		131.9	26.7	0.999	Multistage (4 stages) at constant matric suction = 200 kPa
A1	IHPT92	UD3-92	5.25–5.40	U2-92		197.5	24.0	0.994	Multistage (3 stages) at constant matric suction = 300 kPa
A1	IHPT92	UD4-92	7.00–7.15	S2-92	29.6		26.5	0.997	Multistage (4 stages) at constant matric suction = 0 kPa
B2	IHPT92	UD2-92	3.55–3.70	S3-92	39.0		25.9	0.999	Multistage (4 stages) at constant matric suction = 0 kPa
B2	IHPT92	UD3-92	5.30–5.45	S4-92	44.5		26.5	0.991	Multistage (4 stages) at constant matric suction = 0 kPa

NOTE: Total cohesion $c = c' + (u_a - u_w) \tan \phi'$; $c = c'$ at $(u_a - u_w) = 0$.

soil. Figure 16 shows a typical profile in a residual soil slope. The angle of the slope, α, the location of the groundwater table below the slope surface, H, and other variables are shown in Fig. 16. The potential slip surface is assumed to be parallel to the ground surface. Therefore, a semi-infinite slope analysis can be used to compute the factor of safety of the slope. The shear force mobilized, S_m, at the base of the slice can be calculated using the shear-strength equation given in [1]:

$$[9] \quad S_m = \frac{1}{F_s}[c' + (\sigma_n - u_a)\tan\phi' + (u_a - u_w)\tan\phi^b]\frac{1}{\cos\alpha}$$

where

S_m is shear force mobilized, which is equal to $W \sin \alpha$, where W is the weight of a slice of a unit width;
$(\sigma_n - u_a)$ is net normal stress on the slip surface; and
F_s is factor of safety

Two pore-water pressure conditions are considered here, namely (*i*) a hydrostatic condition (Fig. 16), and (ii) three nonhydrostatic conditions associated with water infiltration into the slope (Fig. 17). Pore-water pressure profile *a* represents the situation where the matric suction is reduced to zero at the ground surface and the suction increases with depth until it reaches the hydrostatic line at depth y_s. Pore-water pressure profile *b* corresponds to the advancement of a wetting front as suggested by Lumb (1962). Pore-water pressure profile *c* is indicative of a perched water table at a depth y_s. By assuming that the pore-air pressure is atmospheric (i.e., $u_a = 0$) and the unit weight of the soil, γ, is constant with depth, the factor of safety for the hydrostatic condition can be written as follows:

$$[10] \quad F_s = \left(\frac{\tan\phi'}{\tan\alpha}\right) + \left(\frac{c'}{\gamma(H-y)}\right)\frac{1}{\sin\alpha\cos\alpha} + \left(\frac{y}{H-y}\right)\left(\frac{\gamma_w}{\gamma}\right)\left(\frac{\tan\phi^b}{\tan\alpha}\right)$$

where

y is height of the slip surface above the groundwater table, and
γ_w is unit weight of water

For the nonhydrostatic conditions, the depth of water infiltration, y_s, is arbitrarily assigned to a value of 5 m. Further percolation of water to a greater depth may be restricted due to the low permeability of the underlying soil. Therefore, the nonhydrostatic conditions can be represented by three possible pore-water pressure profiles as shown in Fig. 17 (Fredlund and Rahardjo 1993*a*). Using the same assumptions as for the hydrostatic condition (i.e., pore-air pressure is atmospheric and the unit weight of soil, γ, is constant with depth), similar analyses can be performed for the nonhydrostatic conditions. The factors of safety corresponding to slip surfaces at a depth of $(H - y) \leq y_s$ can be written for the pore-water pressure profiles as follows. For profile *a*, the factor of safety is

$$[11] \quad F_s = \left(\frac{\tan\phi'}{\tan\alpha}\right) + \left(\frac{c'}{\gamma(H-y)}\right)\frac{1}{\sin\alpha\cos\alpha} + \left(\frac{H}{y_s} - 1\right)\left(\frac{\gamma_w}{\gamma}\right)\left(\frac{\tan\phi^b}{\tan\alpha}\right)$$

For profile *b*, the factor of safety is

Fig. 13. Interpretation of the angle of friction with respect to matric suction, ϕ^b, from the results of multistage triaxial test at a constant net confining pressure.

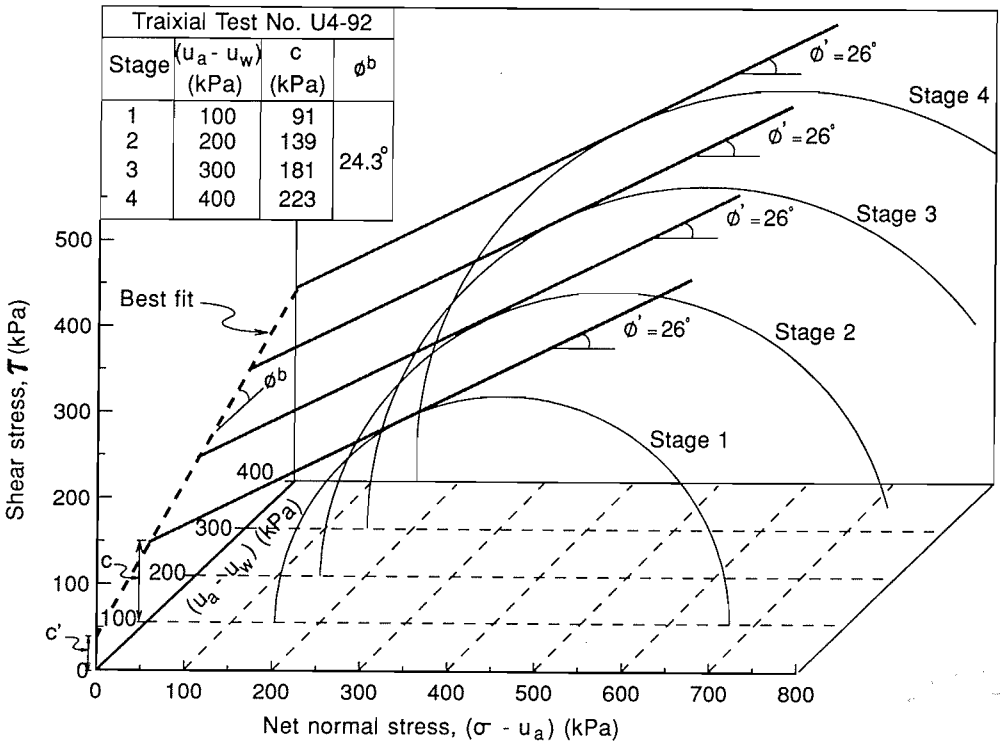

Fig. 14. Intersection lines between the failure envelopes and the shear stress vs. matric suction plane.

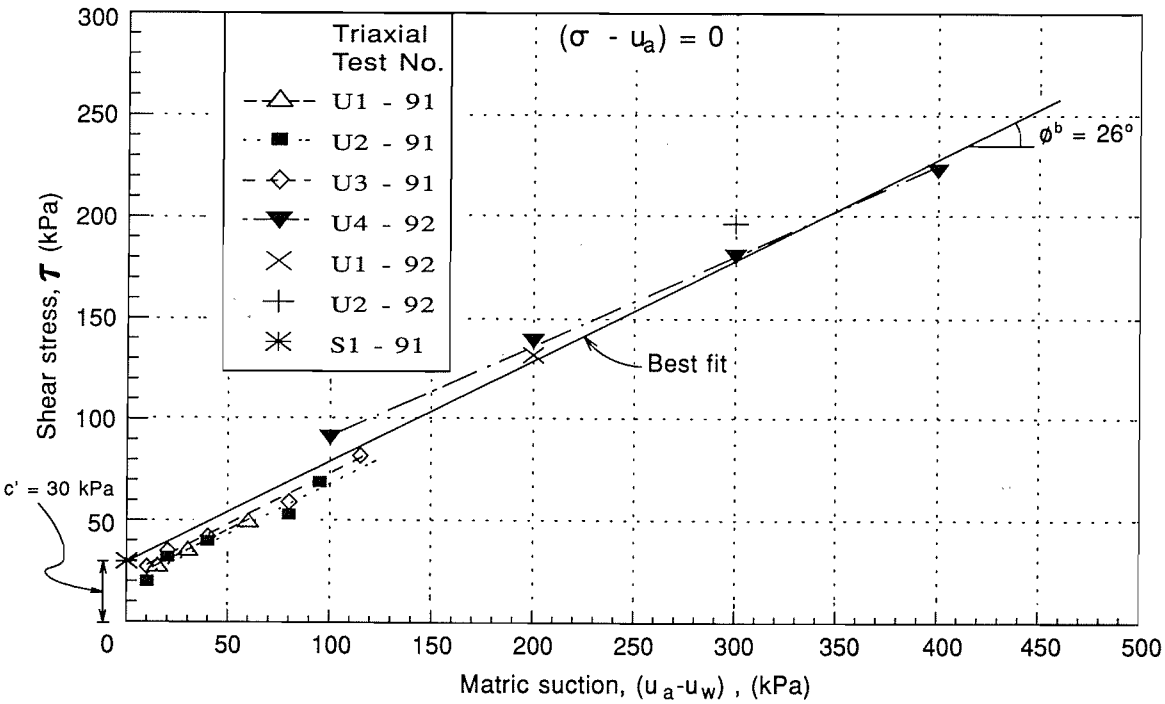

Table 5. Summary of ϕ^b values interpreted from triaxial tests.

Borehole No.	Location	Sample No.	Depth (m)	Triaxial test No.	Shear-strength parameters ϕ' (°)	Shear-strength parameters ϕ^b (°)	Description of test
A1	IHPT91	UD2-91	3.15–3.30	U1-91	26.0	26.4	Multistage (3 stages) at constant net confining pressure = 25 kPa
A1	IHPT91	UD2-91	3.30–3.45	U2-91	26.0	26.5	Multistage (5 stages) at constant net confining pressure = 100 kPa
A1	IHPT91	UD2-91	3.45–3.60	U3-91	26.0	26.5	Multistage (5 stages) at constant net confining pressure = 200 kPa
A1	IHPT92	UD4-91	7.15–7.30	U4-92	26.0	24.3	Multistage (4 stages) at constant net confining pressure = 150 kPa

NOTE: Total cohesion $c = c' + (u_a - u_w) \tan \phi'$; $c = c'$ at $(u_a - u_w) = 0$

Fig. 15. Soil-water characteristic curves of silty clay specimens from the residual soil of the sedimentary Jurong Formation. *e*, void ratio; *S*, degree of saturation.

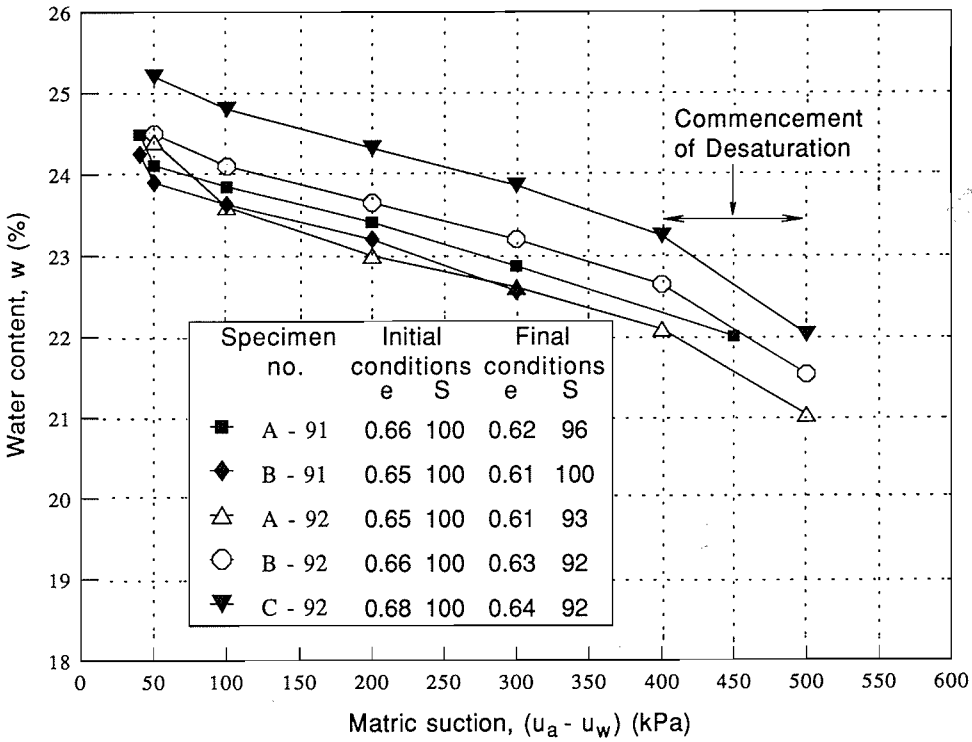

$$[12] \quad F_s = \left(\frac{\tan \phi'}{\tan \alpha}\right) + \left(\frac{c'}{\gamma(H-y)}\right)\frac{1}{\sin \alpha \cos \alpha}$$

For profile *c*, the factor of safety is

$$[13] \quad F_s = \left(\frac{\tan \phi'}{\tan \alpha}\right) + \left(\frac{c'}{\gamma(H-y)}\right)\frac{1}{\sin \alpha \cos \alpha} - \left(\frac{\gamma_w}{\gamma}\right)\left(\frac{\tan \phi^b}{\tan \alpha}\right)$$

Equation 10 can also be used to compute F_s for slip surfaces at a depth of $(H - y) \leq y_s$ under the nonhydrostatic condition.

The calculated factors of safety corresponding to different values of ϕ^b for the hydrostatic condition are shown in Fig. 18. Note that if ϕ^b is assumed equal to 0, there is no account taken of the contribution of suction toward the stability of the slope. It appears that by incorporating matric suction into the analysis, the factor of safety increases with an increase in the ϕ^b value. The increase in the factor of safety can be very significant when the sliding surface is high above the groundwater table.

In the case of water infiltration into the slope, the factor of safety depends on the pore-water pressure profile illustrated in Fig. 19 for a ϕ^b value of 26°. In all cases, the factor of safety decreases most rapidly when the slip surface is near the ground surface (i.e., shallow slides). Theoretically,

Fig. 16. Geometry and definition of variables associated with stability analysis in a residual soil slope.

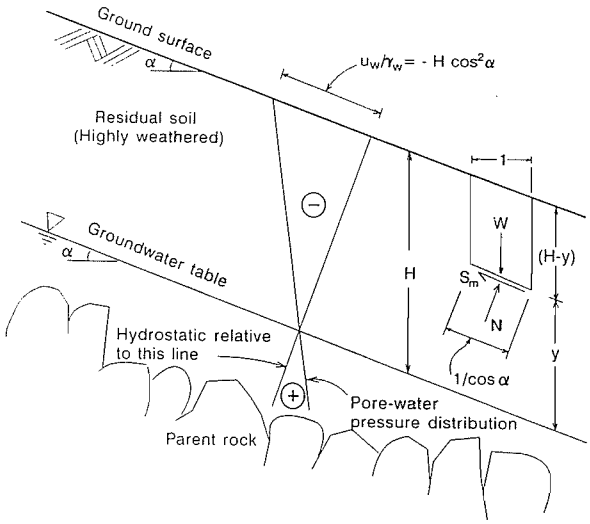

Fig. 17. Three possible pore-water pressure profiles (*a*, *b*, and *c*; see text) in the zone above the groundwater table due to infiltration of water into the slope.

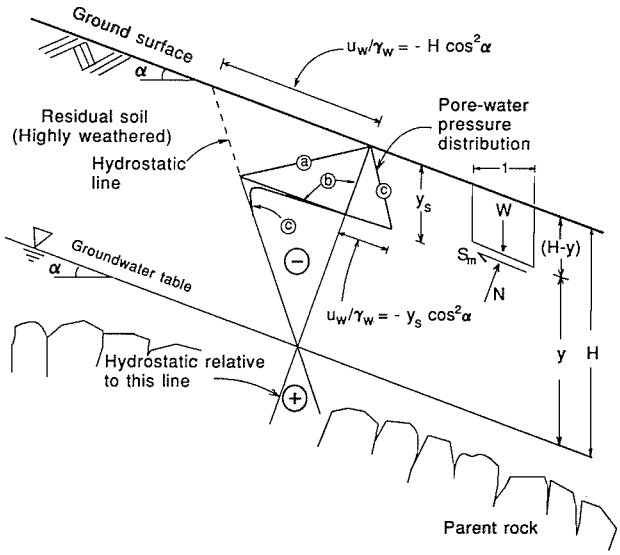

the plane of slippage will occur in the zone where the computed factor of safety is the lowest (i.e., within the wetted zone). However, the actual location of the slip surface will be controlled by the field shear-strength profile.

Conclusions

The residual soil of the Jurong Formation in Singapore shows an increase in shear strength with an increase in matric suction. Multistage consolidated drained triaxial tests conducted on undisturbed samples obtained from two sites indicated similar results. The effective angle of internal friction, ϕ', was found to be equal to 26° while the effective cohesion, c', varied from 30 to 45 kPa. The average angle of friction with respect to matric suction, ϕ^b, was found to be similar to the ϕ' value of 26° for matric

Fig. 18. Computed factors of safety for various ϕ^b values for the hydrostatic condition used in the semi-infinite slope stability analyses.

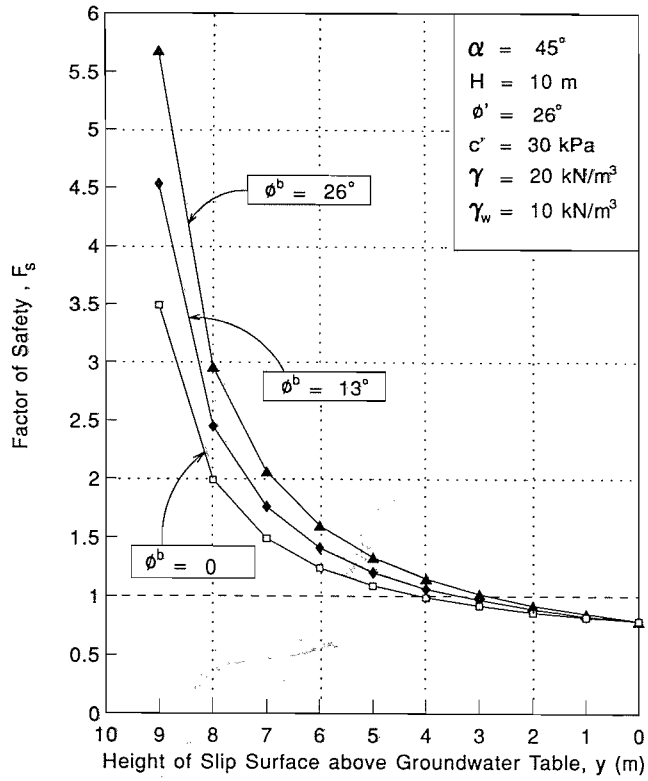

Fig. 19. Computed factors of safety for various pore-water pressure profiles above the groundwater table in the case of water infiltration into the slope.

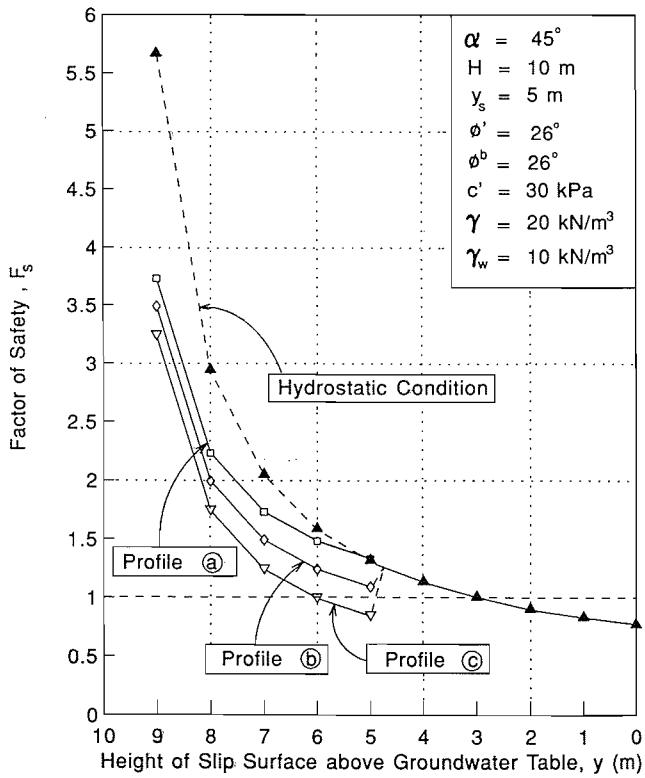

suctions up to 400 kPa. These findings indicate the suitability of using a planar failure envelope for the natural residual soil of the sedimentary Jurong Formation at matric suctions frequently encountered in practice.

The presented examples involving stability analysis of a residual soil slope illustrate the importance of matric suction in slope instability, particularly for shallow slides.

Acknowledgments

The experimental work described in this paper was carried out in the Geotechnics Laboratory of the School of Civil and Structural Engineering, Nanyang Technological University, Singapore. The authors gratefully acknowledge the assistance of Mr. Vincent H. K. Heng of the Geotechnics Laboratory in the experimental program.

References

Brand, E.W. 1984. Landslides in Southeast Asia: A state-of-the-art report. *In* Proceedings, 4th International Symposium on Landslides, Toronto. Vol. 1, pp. 17–59.

Chang, M.F. 1988. In-situ testing of residual soil in Singapore. *In* Proceedings, 2nd International Conference on Geomechanics in Tropical Soils, Singapore. Vol. 1, pp. 97–108.

Fredlund, D.G., and Rahardjo, H. 1985. Theoretical context for understanding unsaturated residual soil behavior. *In* Proceedings, 1st International Conference on Geomechanics in Tropical Lateritic and Saprolitic Soils, Feb., Sao Paulo, Brazil. Vol. 1, pp. 295–305.

Fredlund, D.G., and Rahardjo, H. 1993*a*. The role of unsaturated soil behavior in geotechnical engineering practice. *In* Proceedings, 11th Southeast Asian Geotechnical Conference. *Edited by* S.L. Lee, K.Y. Yong and Y.K. Chow. National University of Singapore, Singapore. pp. 37–49.

Fredlund, D. G., and Rahardjo, H. 1993b. Soil mechanics for unsaturated soils. John Wiley & Sons Inc., New York.

Fredlund, D.G., Morgernstern, N.R., and Widger, R.A. 1978. The shear strength of unsaturated soils. Canadian Geotechnical Journal, **15**: 313–321.

Hilf, J.W. 1956. An investigation of pore pressures in compacted cohesive soils. Technical memorandum 654, U.S. Department of the Interior Bureau of Reclamation, Denver, Colo.

Lambe, T.W., and Whitman, R.V. 1979. Soil mechanics. John Wiley & Sons Inc., New York.

Lim, T.T. 1994. Shear strength characteristics and rainfall-induced matric suction changes in a residual soil slope. M. Eng. thesis, Nanyang Technological University, Singapore.

Lumb, P. 1962. Effect of rain storms on slope stability. *In* Proceedings, Symposium on Hong Kong Soils, Hong Kong, pp. 73–87.

Oyaga, N. 1984. Landslides in weathered rocks and residual soils in Japan and surrounding areas: A state-of-the-art report. *In* Proceedings, 4th International Symposium on Landslides, Toronto. Vol. 3, pp. 1–31.

Pitts, J. 1984. A review of geology and engineering geology in Singapore. Quarterly Journal of Engineering Geology, **17**: 93–101.

Pitts, J. 1985. An investigation of slope stability on the NTI campus, Singapore. Report on Applied Research Project PR1/83, Nanyang Technological Institute, Singapore.

Poh, K.B., Chuah, H.L. and Tan, S.B. 1985. Residual granite soil of Singapore. *In* Proceedings, 8th Southeast Asian Geotechnical Conference, Kuala Lumpur, Malaysia. Vol. 1, pp. 3-1 to 3-9.

Rahardjo, H., and Fredlund, D.G. 1991. Calculation procedure for slope stability analysis involving negative pore-water pressures. *In* Proceedings of International Conference on Slope Stability Engineering Developments and Applications, 15–18 April. The Institution of Civil Engineers, Isle of Wight, pp. 43–49.

Todo, H., and Pauzi, M.M. 1989. Geotechnical engineering properties of residual soils originated from granite in Malaysia and Singapore. *In* Proceedings of the International Conference on Engineering Geology in Tropical Terrains, University of Kebangsaan, Bangi, Malaysia, June 26–29, pp. 160–169.

Vargas, M., and Pichler, E. 1957. Residual soils and rock slides in Santos (Brazil). *In* Proceedings, 4th International Conference on Soil Mechanics and Foundation Engineering, London. Vol. 2, pp. 394–398.

Yong, R.N., Chen, C.K., Sellappah, J., and Chong, T.S. 1985. The characterization of residual soils in Singapore. *In* Proceedings, 8th Southeast Asian Geotechnical Conference, Kuala Lumpur, Malaysia. Vol. 1, pp. 3-19 to 3-26.